Hindawi
Journal of Nanomaterials
Volume 2017, Article ID 1821837, 8 pages
https://doi.org/10.1155/2017/1821837

Research Article

Improving the Efficiency of Dye-Sensitized Solar Cells by Growing Longer ZnO Nanorods on TiO_2 Photoanodes

Bao-gai Zhai, Long Yang, and Yuan Ming Huang

School of Mathematics and Physics, Changzhou University, Jiangsu 213164, China

Correspondence should be addressed to Yuan Ming Huang; dongshanisland@126.com

Received 5 March 2017; Accepted 6 June 2017; Published 9 July 2017

Academic Editor: Zafar Iqbal

By increasing the temperature of hydrothermal reactions from 70 to 100°C, vertically aligned ZnO nanorods were grown on the TiO_2 thin film in the photoanode of dye-sensitized solar cells (DSSCs) as the blocking layer to reduce the electron back recombinations at the TiO_2/electrolyte interfaces. The length effects of ZnO nanorods on the photovoltaic performances of TiO_2 based DSSCs were investigated by means of scanning electron microscope, X-ray diffractometer, photoluminescence spectrophotometer, and the photocurrent-voltage measurement. Under the illumination of 100 mW/cm^2, the power conversion efficiency of DSSC with ZnO nanorods decorated TiO_2 thin film as its photoanode can be increased nearly fourfold from 0.27% to 1.30% as the length of ZnO nanorods increases from 300 to 1600 nm. The enhanced efficiency of DSSC with ZnO nanorods decorated TiO_2 thin film as the photoanode can be attributed to the larger surface area and the lower defect density in longer ZnO nanorods, which are in favor of more dye adsorption and more efficient transport in the photoanode.

1. Introduction

TiO_2 based dye-sensitized solar cells (DSSCs) have been recognized as *the* promising candidates for next-generation solar cells due to their low production cost, low environmental impact, and relatively high power conversion efficiency [1–5]. A typical DSSC consists of a photoanode containing the wide bandgap semiconductor TiO_2, a Pt counter electrode, and a liquid electrolyte containing the I^-/I_3^- redox couple. Under illumination, the dye molecules adsorbed on TiO_2 are excited to their lowest unoccupied molecule orbitals with the result of released photoelectrons, and then the released photoelectrons are injected into the wide bandgap semiconductor TiO_2 [6–9]. Consequently the interface between TiO_2 and the electrolyte becomes critically important in improving the power conversion efficiency of the TiO_2 based DSSCs [6–11]. It is well recognized that a further increase in the power conversion efficiency has been limited by energy loss due to the recombination of electrons in the photoanode with the oxidized dye molecules or with the electron-accepting species in the electrolyte [10–13]. In order to minimize the electron back transfer from TiO_2 to the redox electrolyte, vertically aligned ZnO nanorods are often applied to DSSCs as the blocking layer since they can form an energy barrier at the electrolyte/TiO_2 interface in addition to providing large surface area for dye adsorption and direct pathway for efficient electron transport from the electrolyte to the photoanode [3, 4, 6, 7]. In particular, Wijeratnea and Bandara recently reported that the electron transport and recombination properties of ZnO-based DSSCs depended on the aspect ratio of randomly dispersed ZnO nanorods in the photoanodes [14]. Therefore, the length of vertically aligned ZnO nanorods in the blocking layer can inevitably generate significant impacts on the photovoltaic performances of TiO_2 based DSSCs. However, the length effects of the vertically aligned ZnO nanorods on the power conversion efficiency are not explored for DSSC with ZnO nanorods decorated TiO_2 thin film as its photoanode. For brevity, the photoanode with the structure of ZnO nanorods decorated TiO_2 thin film is shortened as ZnO-TiO_2 photoanode.

In the present work, we investigated the length effects of vertically aligned ZnO nanorods in the ZnO-TiO_2 photoanode on the photovoltaic performance of the DSSC. Vertically aligned ZnO nanorods with tunable lengths ranging from 300 to 1600 nm and diameters of about 75 nm were grown on 600-nm thick TiO_2 thin films by varying the temperature of

hydrothermal reactions from 70 to 100°C. The morphologies, crystal structures, and optical properties of vertically aligned ZnO nanorods were characterized by means of scanning electron microscope (SEM), X-ray diffractometer (XRD), and photoluminescence (PL) spectrophotometer. Our photocurrent-voltage (J-V) measurements under the light illumination of 100 mW/cm^2 demonstrated that the power conversion efficiency of the DSSC with the ZnO-TiO_2 photoanode was enhanced nearly fourfold from 0.27% to 1.30% as the length of ZnO nanorods increased from 300 to 1600 nm.

2. Materials and Methods

2.1. Materials. All of the chemicals used in this study were of analytical grade and were purchased from local chemical suppliers unless mentioned otherwise [3, 6]. Fluorine-doped tin oxide conductive glass (FTO, sheet resistance of about 14 Ω cm^{-2}, thickness 2.2 mm) was used as the electrode substrate. Di-tetrabutylammonium cis-bis (isothiocyanato) bis (2,2′-bipyridyl-4,4′-dicarboxylato) ruthenium (II) (N719) was used as the dye in our DSSCs. The ethanol solution of chloroplatinic acid hexahydrate was used to prepare the counter electrodes.

2.2. TiO_2 Thin Films. The TiO_2 thin film in the photoanode consisted of a compact TiO_2 layer (50 nm) and a porous TiO_2 layer (550 nm) on FTO glass substrate. The compact TiO_2 layer was formed on the FTO glass substrate after having been immersed into an aqueous solution of $TiCl_4$ (0.04 M) at 70°C for 30 min and subsequently sintered at 450°C for 30 min. The porous TiO_2 layer was deposited on the compact TiO_2 layer by dipping the FTO substrates into TiO_2 sol for 10 min and then calcinating at 450°C for 2 h (5 cycles). The TiO_2 sol was a mixture of tetrabutyl titanate (4 mL), diethanolamine (2 mL), deionized water (1.5 mL), acetate acid (1.2 mL), polyethylene glycol (PEG-2000, 0.045 g), and butyl alcohol (60 mL) that had been aged for 16 h. Details on preparing the TiO_2 photoanodes were described in our recent work [3, 4, 6].

2.3. Decoration of the TiO_2 Thin Film with ZnO Nanorods. ZnO nanorods were grown vertically onto the TiO_2 photoanode via the hydrothermal route: (i) ZnO seeding solution was prepared by dissolving zinc acetate dehydrate (6.6 g) and ethanolamine (1.8 mL) into ethanol (60 mL); (ii) one ZnO seed layer was formed on the TiO_2 thin film by dipping the photoanode into the ZnO seeding solution for about 1 min and then drying at 300°C for 10 min (3 cycles); (iii) the ZnO coated TiO_2 thin film was loaded into a Teflon-lined stainless steel autoclave for reaction at a specific temperature for 5 h. The solution in the autoclave was the aqueous solution of zinc nitrate (0.05 M) and hexamethylenetetramine (0.05 M). Four kinds of ZnO nanorods with different lengths were obtained by setting the temperatures in the autoclave at 70, 80, 90, and 100°C, respectively.

2.4. DSSC Assembling. The ZnO-TiO_2 photoanodes were dye-sensitized by immersing them into the ethanol solution of the N719 dye (0.4 mM) for 20 min. Each dye-sensitized photoanode was assembled with a Pt counter electrode into a sandwiched structure with a 25-μm thick sealing spacer between them. The Pt counter electrode was prepared by immersing one piece of cleaned FTO substrate in an ethanol solution of H_2PtCl_6 (4 mM) and then annealing it at 450°C for 2 h. The free space in the sandwiched structure was filled with a redox liquid electrolyte. The electrolyte was the acetonitrile solution of KI (0.5 M) and I_2 (0.05 M).

2.5. Characterizations. A SEM (Hitachi S-4800, Japan) was employed to characterize the morphologies of the ZnO-TiO_2 photoanodes. The crystal structures of the ZnO nanorods were analyzed by XRD (D/max 2500 PC, Rigaku, Japan) with a copper target radiation. The PL spectra of samples were recorded with a spectrophotometer. The 325 nm laser line from a helium-cadmium laser was employed as excitation source for the PL measurement. The output power of ultraviolet laser was about 12 mW. For the J-V measurement of the DSSCs, an AM 1.5 solar simulator with a 500 W xenon lamp was employed to illuminate the DSSC; the incident light power on the solar cells was calibrated to 100 mW/cm^2. The active area of each solar cell was 0.25 cm^2. Other parameters on the instrumentation were available elsewhere [3, 4, 6, 15–17]. The nanostructures of the ZnO-TiO_2 photoanode were characterized with a transmission electron microscope (TEM) (JEOL JEM-2100, Japan Electronics Corp) which was operated at 200 kV.

3. Results and Discussion

Figure 1 shows the top-view and cross-sectional SEM micrographs of the prepared ZnO-TiO_2 photoanodes. The panels (A)–(D) in Figure 1(a) represent the cross-sectional SEM micrographs of the ZnO-TiO_2 photoanodes grown at (A) 70°C, (B) 80°C, (C) 90°C, and (D) 100°C for 5 h. It can be seen clearly that the ZnO nanorods were vertically grown onto the TiO_2 thin films. The average lengths of the ZnO nanorods were 300, 800, 1400, and 1600 nm when the growth temperatures were 70, 80, 90, and 100°C, respectively. The panels (E)–(H) in Figure 1(b) display the top-view SEM micrographs of the ZnO-TiO_2 photoanodes grown at (A) 70°C, (B) 80°C, (C) 90°C, and (D) 100°C for 5 h, respectively. These top-view SEM micrographs illustrate that the vertically aligned ZnO nanorods are densely populated on the TiO_2 thin films. The average diameters of ZnO nanorods are about 75 nm, regardless of the differences in the growth temperatures. Thus, the aspect ratios of the ZnO nanorods are 4.0, 10.7, 18.7, and 21.3 when the growth temperatures were 70, 80, 90, and 100°C, respectively. Moreover, the thickness of the TiO_2 layer, which is around 600 nm, can be estimated from the SEM micrographs in Figure 1. Further TEM and selected area electron diffraction analyses reveal that these ZnO nanorods are single crystalline [16, 17]. Consequently, the data in Figure 1 have demonstrated that vertically aligned ZnO nanorods with lengths varying from 300 to 1600 nm are onto the TiO_2 thin films as the hydrothermal growth temperature increases from 70 to 100°C. The larger surface area provided by longer ZnO nanorods is helpful for more dye adsorption.

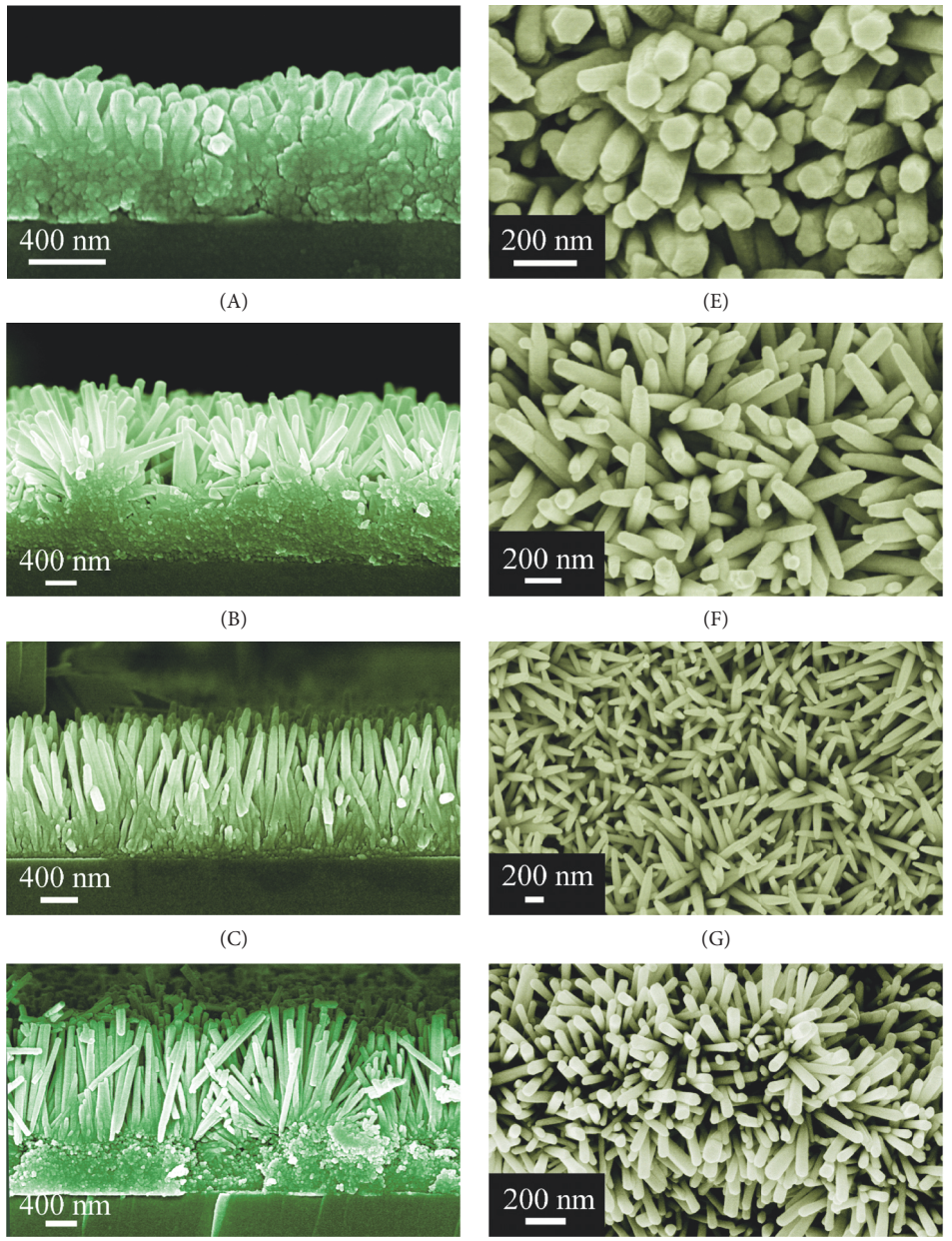

FIGURE 1: (a) Cross-sectional SEM micrographs of the ZnO-TiO_2 photoanodes grown at (A) 70°C, (B) 80°C, (C) 90°C, and (D) 100°C. (b) Top-view SEM micrographs of the ZnO-TiO_2 photoanodes grown at (E) 70°C, (F) 80°C, (G) 90°C, and (H) 100°C.

Figure 2 shows the XRD spectra of the ZnO-TiO_2 photoanodes grown at (a) 70°C, (b) 80°C, (c) 90°C, and (d) 100°C, respectively. The diffraction peaks at 2θ = 31.6, 34.2, 36.0, 47.4, 56.5, 62.8, and 67.8 in each XRD spectrum can be assigned to the reflections from the (100), (002), (101), (102), (110), (103), and (112) planes of the hexagonal ZnO, whose standard lattice constants are a = 0.325 nm and c = 0.521 nm, according to the Joint Committee on Powder Diffraction Standard (JCPDF number 36-1451) [3, 4, 6, 17]. It is noted that the (002) peak at 2θ = 34.2° becomes much more dominant in intensity as the growth temperature gets higher, indicating the enhanced directional order of the ZnO nanorods formed at higher temperature. According to the diffraction equations, the lattice constants a and c can be calculated for the ZnO nanorods grown at different temperatures. Our calculated lattice constants, which are very close to those of wurtzite ZnO, are summarized in Table 1. Additionally, it is well established that the degree of orientation of ZnO nanocrystals can be evaluated by the texture coefficients (TCs), which is defined by the following equation [22]:

$$\mathrm{TC}_{(hkl)} = \frac{I_{(hkl)}/I^{o}_{(hkl)}}{(1/N)\sum I_{(hkl)}/I^{o}_{(hkl)}}, \quad (1)$$

Table 1: Parameters of ZnO nanorods and the photovoltaic parameters of ZnO nanorods decorated DSSCs.

Growth temp (°C)	Length (nm)	Diameter (nm)	a (nm)	c (nm)	J_{sc} (mA/cm^2)	V_{oc} (V)	η (%)	FF
No decoration	na	na	na	na	0.37	0.66	0.15	0.614
70	300	75	0.327	0.523	0.92	0.61	0.27	0.481
80	1000	75	0.326	0.522	1.60	0.59	0.56	0.594
90	1400	75	0.327	0.523	2.70	0.56	0.84	0.555
100	1600	75	0.326	0.522	4.23	0.55	1.30	0.559

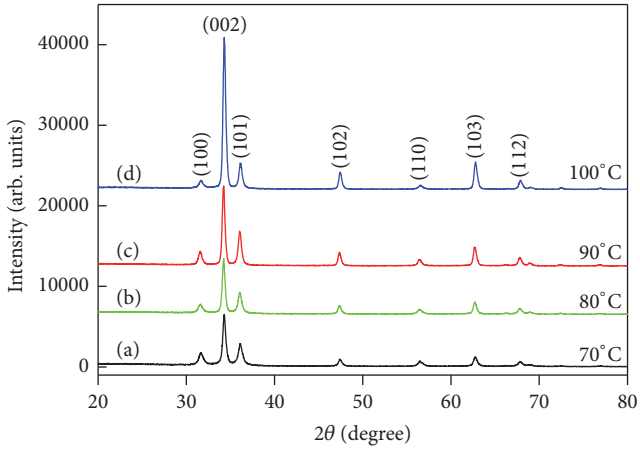

Figure 2: XRD spectra of the ZnO-TiO_2 photoanodes grown at (a) 70°C; (b) 80°C; (c) 90°C; and (d) 100°C.

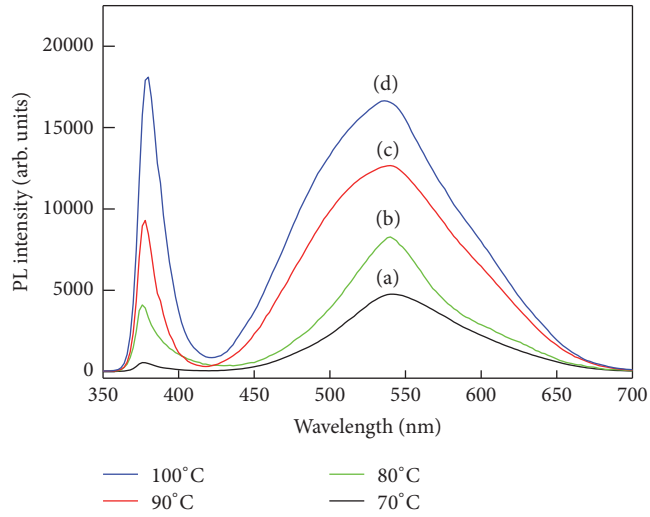

Figure 3: PL spectra of ZnO-TiO_2 photoanodes grown at (a) 70°C; (b) 80°C; (c) 90°C; and (d) 100°C.

where N is the number of diffraction peaks, $I_{(hkl)}$ is the experimentally measured intensity of the diffraction peak (hkl), and $I^o_{(hkl)}$ is the recorded intensity of the (hkl) diffraction peak according to the JCPDS 036-1451 card. According to (1), the TCs for the (002) orientations were calculated to be 3.30, 3.453, 3.585, and 4.20 for the ZnO nanorods grown at 70, 80, 90, and 100°C, respectively. The higher $TC_{(002)}$ value shows that the ZnO nanorods are more perfectly aligned with their c-axis perpendicular to the substrate. Therefore, the data in Figure 2 has given further evidence on the formation of hexagonal ZnO nanorods and their perpendicular alignment on the substrates.

Figure 3 illustrates the room temperature PL spectra of the ZnO-TiO_2 photoanodes grown at (a) 70°C, (b) 80°C, (c) 90°C, and (d) 100°C, respectively. It is obvious that each PL spectrum in Figure 3 consists of an ultraviolet PL band with its peak at about 378 nm and a green PL band with its peak at about 540 nm. The ultraviolet PL band is generally attributed to the band-edge recombination of excitons whereas the green PL band is produced by defects in ZnO [15–17, 22–25]. Therefore, the higher fraction of the green PL intensity in the PL spectrum suggests the presence of higher defect density in ZnO nanorods. On the basis of the PL data in Figure 3, the fractions of the green PL intensity in the PL spectra are derived to be 0.9768, 0.9061, 0.8958, and 0.8479 for the PL curves (a)–(d), respectively. So, lower defect density is present in ZnO nanorods when growth temperature gets higher. Combined to the results in Figure 2, it is obvious that the lower defect density in longer ZnO nanorods is good for more efficient electron transport in the nanorods.

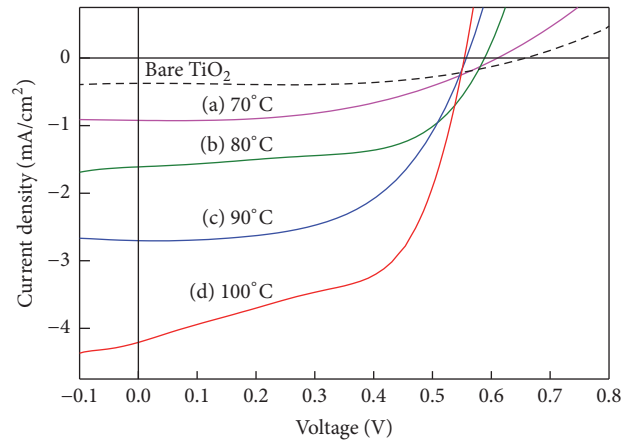

Figure 4: J-V curves of DSSCs with ZnO-TiO_2 photoanodes grown at different temperatures: (a) 70°C; (b) 80°C; (c) 90°C; and (d) 100°C.

Figure 4 presents the J-V curves of DSSCs with the ZnO-TiO_2 photoanodes grown at different temperatures, (a) 70°C, (b) 80°C, (c) 90°C, and (d) 100°C. The J-V curve of the DSSC without the decoration of ZnO nanorods is shown in Figure 4 as a reference (dashed line). All the J-V curves were measured under the illumination of one sun

(100 mW/cm^2). The photovoltaic performance parameters of the DSSCs, that is, the short-circuit current density (J_{SC}), open-circuit voltage (V_{OC}), filling factor (FF), and power conversion efficiency (η), are summarized in Table 1. It can be seen in both Figure 4 and Table 1 that the length of vertically aligned ZnO nanorods generates a significant effect on the photovoltaic performance of the DSSCs. As the length of the ZnO nanorods increases from 300 to 1600 nm, the J_{SC} of the DSSCs increases from 0.92 to 4.23 mA/cm^2, in the meanwhile the V_{OC} of the DSSCs decreases slightly from 0.61 to 0.55 V, yielding the overall efficiency of the DSSCs of 0.27, 0.56, 0.84, and 1.30%, respectively. In contrast, those parameters for the DSSC without ZnO decoration are 0.37 mA/cm^2, 0.66 V, and 0.15%, respectively. The improved photovoltaic performance of DSSCs can be attributed to the following facts: (i) an energy barrier is formed at the TiO_2/electrolyte interface to reduce the electron back recombination [3, 4, 6–10]; (ii) the longer ZnO nanorods provide larger surface area for more dye adsorption; and (iii) the lower defect density in longer ZnO nanorods favors more efficient electron transport in the nanorods. More specifically, the enhancement in J_{SC} can be attributed to the larger surface area and the lower defect density in longer ZnO nanorods whilst the slight decrease in V_{OC} can be caused by the larger serial resistance in the longer ZnO nanorods. Therefore, the data in Figure 4 have demonstrated that growing longer ZnO nanorods on TiO_2 thin films can effectively enhance the efficiency of the DSSCs. The presented data in Figure 4 were reproduced in four batches of solar cells; each batch consisted of one DSSC without the decoration of ZnO nanorods and four DSSCs with the ZnO-TiO_2 photoanodes. The statistical derivations of the efficiency were found to be within ±7% for the samples.

The solar power conversion efficiencies of DSSCs with conventional TiO_2 photoanodes were routinely reported to be more than 5% even without any scattering layer or blocking layer [1, 2, 5]. It is well established that the solar power conversion efficiency of conventional TiO_2 based DSSCs heavily depends on the thickness of the TiO_2 photoanode [26, 27], and that very thick TiO_2 photoanodes (10–20 μm) are routinely employed to achieve high efficiency up to 12%. For example, Wu et al. reported the efficiency of 8.19% when the TiO_2 film was 20 μm thick [26]. As shown in Figure 1, the thickness of our sol-gel derived TiO_2 layer is only about 0.6 μm. That is the reason why our TiO_2 based DSSC has a very low efficiency of 0.15%. Since it is hard to make thick TiO_2 films via the sol-gel process, we employed the doctor blade technique to prepare 15 μm thick TiO_2 photoanodes for the DSSCs. Our measured efficiency of the thick TiO_2 based DSSCs without the decoration of ZnO nanorods was 4.3% whilst the efficiency of the thick TiO_2 based DSSCs with the decoration of vertically aligned ZnO nanorods (1 μm thick) reached up to 9.8%. Compared to the thick TiO_2 films made with the doctor blade technique, the thin TiO_2 films grown via the sol-gel process exhibit the advantages of uniform thickness of the film, no cracks in the films, and very good reproducibility in the solar power conversion efficiency for the TiO_2 based DSSCs. In order to derive a reliable relationship between the efficiency of the DSSCs and the length of ZnO nanorods, we have chosen sol-gel derived thin TiO_2 films as the first layer in the photoanodes of our DSSCs. Surely there are several other major areas for improvement before we can have a comprehensive understanding on ZnO nanorods decorated DSSCs.

Both the morphology and the size of the nanostructured crystallites are important factors to influence the solar power conversion efficiency of DSSC with the ZnO-TiO_2 photoanode. We derived the ZnO nanorods and the TiO_2 nanoparticles from the photoanode by scratching the photoanode with a blade plus ultrasonicating in water for 30 min. Figure 5(a) displays the high-resolution TEM micrograph of a piece of TiO_2 thin film derived from the ZnO-TiO_2 photoanode. It can be seen clearly in Figure 5(a) that the piece of TiO_2 thin film consists of numerous TiO_2 nanoparticles whose sizes are in the range of 3–10 nm. The inset in Figure 5(a) represents the crystal lattice of one TiO_2 nanoparticle. As shown by the inset, the lattice spacing of (101) crystallographic plane is around 0.352 nm. Figure 5(b) shows the selected area electron diffraction pattern of TiO_2 nanoparticles derived from the ZnO-TiO_2 photoanode. The bright spots in Figure 5(b) give evidence on the crystalline nature of the TiO_2 nanoparticles in the photoanode. Figure 5(c) depicts the low resolution TEM micrograph of ZnO nanorods derived from ZnO-TiO_2 photoanode. It is observed in Figure 5(c) that both long and short ZnO nanorods are present. The lengths of the long ZnO nanorods are around 300 nm with their diameters of around 20 nm. The short ZnO nanorods in Figure 5(c) are believed to be the broken fragments of long ZnO nanorods when they are scratched off the photoanode.

The quality of the interface between ZnO nanorods and the TiO_2 nanoparticles is another critical parameter to influence the solar power conversion efficiency of DSSC with the ZnO-TiO_2 photoanode. Hence it would be better to display the cross-sectional view of TEM image of the interface between ZnO and TiO_2. However, it is rather difficult to prepare high quality samples for high-resolution TEM characterization since ultrasonication introduced shock wave breaks TiO_2 nanoparticles away from ZnO nanorods. As a compensation, we characterized the ZnO-TiO_2 interface with SEM. Figure 6 shows the cross-sectional SEM micrographs of the ZnO-TiO_2 interface in the photoanode: (a) the ZnO-TiO_2 interface whose ZnO nanorods were grown at 70°C; (b) an enlarged section of the ZnO-TiO_2 interface whose ZnO nanorods were grown at 70°C; and (c) free-standing ZnO-TiO_2 interface whose ZnO nanorods were grown at 80°C. It is clear that ZnO nanorods are grown vertically on the top surface of the TiO_2 thin film, no matter the TiO_2 thin film is smooth or rough.

As stated in the Introduction, the length effects of vertically aligned ZnO nanorods on the power conversion efficiency of DSSC with the ZnO-TiO_2 photoanode were not reported in the literature. Although Wijeratne and Bandara studied the aspect ratio effect of ZnO nanorods on the electron transport and recombination properties of ZnO-based

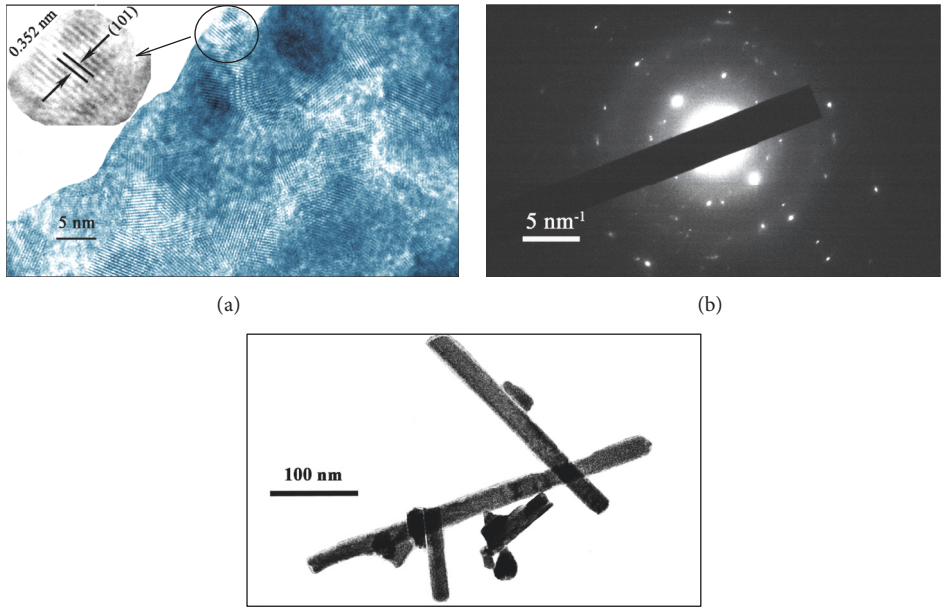

FIGURE 5: (a) High-resolution TEM micrograph of TiO_2 derived from the ZnO-TiO_2 photoanode. (b) Selected area electron diffraction pattern of TiO_2 nanoparticles derived from the ZnO-TiO_2 photoanode. (c) Low resolution TEM micrograph of ZnO nanorods derived from the ZnO-TiO_2 photoanode.

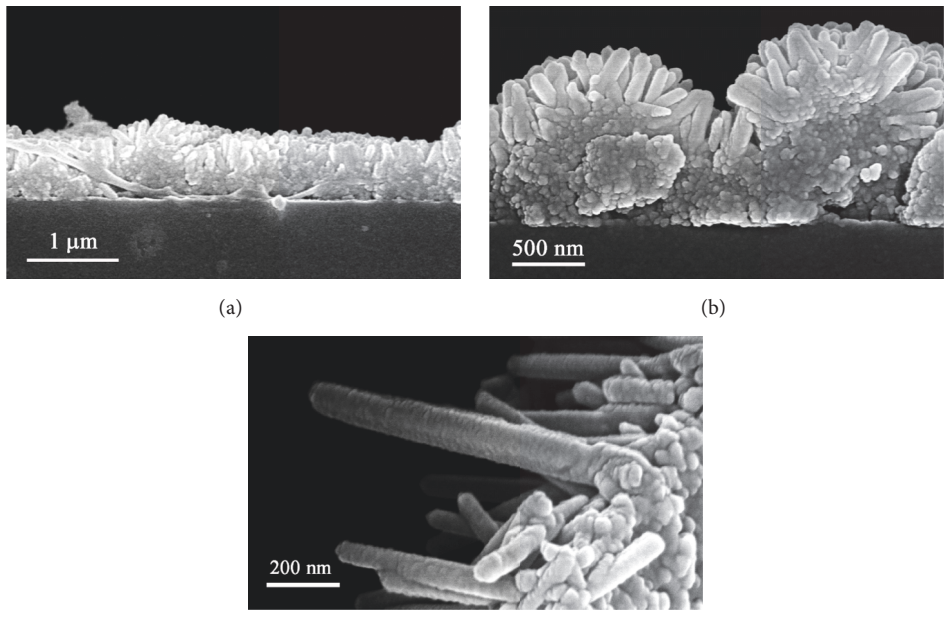

FIGURE 6: Cross-sectional SEM micrographs of the ZnO-TiO_2 interface in the photoanode: (a) the ZnO-TiO_2 interface whose ZnO nanorods were grown at 70°C; (b) an enlarged section of the ZnO-TiO_2 interface whose ZnO nanorods were grown at 70°C; and (c) free-standing ZnO-TiO_2 interface whose ZnO nanorods were grown at 80°C.

DSSCs, their photoanodes were composed of ZnO nanorods only [14]. Table 2 lists the photovoltaic performance parameters of the DSSCs with different photoanode structures. It is obvious in Table 2 that the photoanode with the structure of ZnO nanorods decorated TiO_2 thin film is more efficient than those with the structures of TiO_2-ZnO core-shell nanograss [18], TiO_2-decorated ZnO nanorod [19], and composite ZnO/TiO_2 (90/10) [20], although less efficient than the

Table 2: Comparison of the performance parameters of the DSSCs with different photoanode structures.

Structure of photoanode	Aspect ratio of ZnO nanorods	η (%)	Reference
ZnO nanorods decorated TiO_2 thin film	21.3	1.30	This work
TiO_2-ZnO core-shell nanograss	na	0.62	[18]
TiO_2-decorated ZnO nanorod	na	0.93	[19]
Composite ZnO/TiO_2 (90/10)	na	0.81	[20]
ZnO/TiO_2 nanonetwork	na	1.60	[21]

photoanode with the structure of ZnO/TiO_2 nanonetwork [21].

4. Conclusion

By increasing the temperature of hydrothermal reactions from 70 to 100°C, we have grown vertically aligned ZnO nanorods onto the TiO_2 photoanodes as the blocking layer in DSSCs to reduce the electron back transfer at the TiO_2/electrolyte interfaces. The length of ZnO nanorods is tunable from 300 to 1600 nm as the hydrothermal reaction temperature increases from 70 to 100°C. The length effects of the ZnO nanorods on the photovoltaic performances of DSSC with the ZnO-TiO_2 photoanode have been investigated. The J-V measurement under the light illumination of 100 mW/cm^2 has demonstrated that the power conversion efficiency of DSSC with the ZnO-TiO_2 photoanode can be increased from 0.27% to 1.30% as the length of ZnO nanorods increases from 300 to 1600 nm. The nearly fourfold enhancement in the efficiency of the ZnO nanorods decorated DSSCs can be attributed to the larger surface area and the lower defect density in longer ZnO nanorods. Our results suggest that a high surface area of the nanostructured ZnO blocking layer is essential to realize highly efficient DSSC because it allows adsorption of sufficiently large number of dye molecules for efficient light harvesting. As a result, the efficiency of TiO_2 based DSSC can be effectively enhanced by growing long ZnO nanorods on the TiO_2 photoanode.

Conflicts of Interest

The authors declare that they have no conflicts of interest.

Acknowledgments

This work was supported by the Natural Science Foundation of China under Grant nos. 11574036 and 11604028.

References

[1] B. O'Regan and M. Grätzel, "A low-cost, high-efficiency solar cell based on dye-sensitized colloidal TiO_2 films," *Nature*, vol. 353, pp. 737–740, 1991.

[2] C.-S. Chou, Y.-T. Kuo, J.-W. Jhang, and P. Wu, "Bi-functional lithium doping in dye-sensitized solar cells," *Solar Energy*, vol. 109, no. 1, pp. 111–117, 2014.

[3] L. Yang, Q.-L. Ma, Y. Cai, and Y. M. Huang, "Enhanced photovoltaic performance of dye sensitized solar cells using one dimensional ZnO nanorod decorated porous TiO_2 film electrode," *Applied Surface Science*, vol. 292, pp. 297–300, 2014.

[4] Q.-L. Ma and Y. M. Huang, "Improved photovoltaic performance of dye sensitized solar cell by decorating TiO_2 photoanode with Li-doped ZnO nanorods," *Materials Letters*, vol. 148, pp. 171–173, 2015.

[5] Q. Zhang, C. S. Dandeneau, S. Candelaria et al., "Effects of lithium ions on dye-sensitized ZnO aggregate solar cells," *Chemistry of Materials*, vol. 22, no. 8, pp. 2427–2433, 2010.

[6] L. Yang, B.-G. Zhai, Q.-L. Ma, and Y. M. Huang, "Effect of ZnO decoration on the photovoltaic performance of TiO_2 based dye sensitized solar cells," *Journal of Alloys and Compounds*, vol. 605, pp. 109–112, 2014.

[7] S.-S. Kim, S.-I. Na, and Y.-C. Nah, "TiO_2 nanotubes decorated with ZnO rod-like nanostructures for efficient dye-sensitized solar cells," *Electrochimica Acta*, vol. 58, pp. 503–509, 2011.

[8] R. Harikisun and H. Desilvestro, "Long-term stability of dye solar cells," *Solar Energy*, vol. 85, no. 6, pp. 1179–1188, 2011.

[9] H. Choi, C. Nahm, J. Kim et al., "The effect of $TiCl_4$-treated TiO_2 compact layer on the performance of dye-sensitized solar cell," *Current Applied Physics*, vol. 12, no. 3, pp. 737–741, 2012.

[10] R. Liu, W.-D. Yang, L.-S. Qiang, and H.-Y. Liu, "Conveniently fabricated heterojunction ZnO/TiO_2 electrodes using TiO_2 nanotube arrays for dye-sensitized solar cells," *Journal of Power Sources*, vol. 220, pp. 153–159, 2012.

[11] K. M. Lee, E. S. Lee, B. Yoo, and D. H. Shin, "Synthesis of ZnO-decorated TiO_2 nanotubes for dye-sensitized solar cells," *Electrochimica Acta*, vol. 109, pp. 181–186, 2013.

[12] E. Gondek, Y. Djaoued, J. Robichaud et al., "Influence of TiO_2 nanoparticles on the photovoltaic efficiency of the ITO/PEDOT:PSS/fluorine copolymers/polythiophene: TiO_2/Al architecture," *Journal of Materials Science: Materials in Electronics*, vol. 23, no. 11, pp. 2057–2064, 2012.

[13] M. K. Nazeeruddin, E. Baranoff, and M. Grätzel, "Dye-sensitized solar cells: a brief overview," *Solar Energy*, vol. 85, no. 6, pp. 1172–1178, 2011.

[14] K. Wijeratne and J. Bandara, "Aspect-ratio dependent electron transport and recombination in dye-sensitized solar cells fabricated with one-dimensional ZnO nanostructures," *Electrochimica Acta*, vol. 148, no. 1, pp. 302–309, 2014.

[15] Q. L. Ma, R. Xiong, B.-G. Zhai, and Y. M. Huang, "Ultrasonic synthesis of fern-like ZnO nanoleaves and their enhanced photocatalytic activity," *Applied Surface Science*, vol. 324, pp. 842–848, 2015.

[16] Y. M. Huang, Q.-L. Ma, and B.-G. Zhai, "A simple method to grow one-dimensional ZnO nanostructures in air," *Materials Letters*, vol. 93, pp. 266–268, 2013.

[17] Y. M. Huang, Q.-L. Ma, and B.-G. Zhai, "Controlled morphology of ZnO nanostructures by adjusting the zinc foil heating temperature in an air-filled box furnace," *Materials Chemistry and Physics*, vol. 147, no. 3, pp. 788–795, 2014.

[18] S. A. M. Samsuri, M. Y. A. Rahman, A. A. Umar, and M. M. Salleh, "Effect of ZnO growth time on the performance of dye-sensitized solar cell utilizing TiO_2-ZnO core–shell nanograss hetero-structure," *Materials Letters*, vol. 160, pp. 388–391, 2015.

[19] T. Guo, Y. Chen, L. Liu et al., "Enhanced photovoltaic performance of dye-sensitized solar cells using TiO_2-decorated ZnO nanorod arrays grown on zinc foil," *Journal of Power Sources*, vol. 201, pp. 408–412, 2012.

[20] M. Giannouli, "Nanostructured ZnO, TiO_2, and composite ZnO/TiO_2 films for application in dye-sensitized solar cells," *International Journal of Photoenergy*, vol. 2013, Article ID 612095, 8 pages, 2013.

[21] A. Vomiero, I. Concina, M. M. Natile et al., "ZnO/TiO_2 nanonetwork as efficient photoanode in excitonic solar cells," *Applied Physics Letters*, vol. 95, no. 19, Article ID 193104, 2009.

[22] O. Lupan, V. M. Guérin, I. M. Tiginyanu et al., "Well-aligned arrays of vertically oriented ZnO nanowires electrodeposited on ITO-coated glass and their integration in dye sensitized solar cells," *Journal of Photochemistry and Photobiology A: Chemistry*, vol. 211, no. 1, pp. 65–73, 2010.

[23] M. D. McCluskey and S. J. Jokela, "Defects in ZnO," *Journal of Applied Physics*, vol. 106, no. 7, Article ID 071101, 2009.

[24] Y. M. Huang, Q.-L. Ma, and B.-G. Zhai, "Core-shell Zn/ZnO structures with improved photocatalytic properties synthesized by aqueous solution method," *Functional Materials Letters*, vol. 6, no. 6, Article ID 1350058, 2013.

[25] Q.-L. Ma, R. Xiong, B.-G. Zhai, and Y. M. Huang, "Core-shelled Zn/ZnO microspheres synthesised by ultrasonic irradiation for photocatalytic applications," *Micro and Nano Letters*, vol. 8, no. 9, pp. 491–495, 2013.

[26] X. Wu, G. Lu, and L. Wang, "The effect of photoanode thickness on the performance of dye-sensitized solar cells containing TiO_2 nanosheets with exposed reactive {001} facets," *Journal of Materials Research*, vol. 28, no. 3, pp. 475–479, 2013.

[27] S. Ito, T. N. Murakami, P. Comte et al., "Fabrication of thin film dye sensitized solar cells with solar to electric power conversion efficiency over 10%," *Thin Solid Films*, vol. 516, no. 14, pp. 4613–4619, 2008.